Mechanical activation of cells induces chromatin remodelling preceding MKL nuclear transport

K.Venkatesan Iyer[†,‡], S. Pulford[§], A. Mogilner[§,ǂ] &G.V. Shivashankar[†,□,*]

[†]Mechanobiology Institute, National University of Singapore, Singapore – 117411

[□]Department of Biological Sciences, National University of Singapore, Singapore – 117543

[‡]National Centre for Biological Sciences, Tata Institute of Fundamental Research, Bangalore - 560065, India

[§]Department of Neurobiology, Physiology and Behaviour, University of California, Davis, CA-95616

[ǂ]Department of Mathematics, University of California, Davis, CA-95616

[*]Corresponding Author:

G.V.Shivashankar

Mechanobiology Institute, National University of Singapore, Singapore – 117411

E-mail: shiva.gvs@gmail.com

Supporting Information

Supporting Methods

Force calibration

Calibration of the electromagnet was performed using 4 μm (diameter) paramagnetic beads (Micromod Partikeltechnologie GmbH, Germany). The beads were suspended in 96% glycerol solution (96% Glycerol, 4% beads in MilliQ water, V/V) and loaded on a 22 X 40 coverslip. The electromagnet was positioned ~ 50 μm from the surface of the coverslip using a motorized 3-axis actuator (Newport Corp, USA) and a current of 1.5 A was passed through the electromagnet using a regulated DC power supply (Good Will Instrument, Taipei, Taiwan**)** to generate the magnetic field. Fast time lapse images of the beads were acquired using a 20X objective on Nikon Eclipse Ti microscope equipped with an EMCCD (Andor Technology, USA). The beads were tracked using an ImageJ plugin MTrackJ (http://rsbweb.nih.gov/ij/index.html) and velocity of the bead at different distances from the electromagnet was computed (Fig. S6). Force on each 4 μm bead was estimated using Stokes law, $F = 6\pi\eta rv$, where η is the viscosity of 96% glycerol solution (624 mPa.s), r is the radius of the bead and v is the velocity of the bead. The force on individual 100 nm (diameter) paramagnetic beads was estimated by scaling the force on the 4μm bead by a factor of the ratio between the magnetization of the 100 nm bead (m_{100}) and the 4 μm bead (m_{4000}). The force is given by:

$$F_{100}(x) = \frac{m_{100}}{m_{4000}} F_{4000}(x)$$

where *x* denotes the distance from the electromagnet and F_{100} and F_{4000} are the forces on 100 nm and 4 μm beads respectively. To estimate the total number of beads adhered on the plasma membrane, cells were incubated with 100 nm fluorescent carboxyl beads (Molecular Probes, Life Technologies, USA) for 2 hours and confocal Z sections were acquired. The number of beads adhered on the membrane was estimated using IMARIS (Bitplane, Switzerland) (Fig. S5). The mean number of beads, N was used to calculate the force on each cell as:

$$F_{cell}(x) = N.F_{100}(x)$$

The force estimated from the above equation after putting the values of N and F_{100}(30 μm) was 1.25 nN

Immunofluorescence staining

Cells grown on coverslip bottomed dishes or coverslips were fixed with 4% paraformaldehyde (PFA) for 15 min followed by 15 min of permeabilization with 0.5 % Triton X-100. Cells were washed twice with 1X PBS for removal of Triton X-100 and was followed by blocking in 1% BSA for 30 min. Cells were then incubated in primary antibody diluted in 1% BSA, for 1 hour. This was followed with washing with 1X PBS and incubation in secondary antibody (diluted in 1% BSA) for 1 hour. Cells were then washed with 1X PBS and stored in PBS or mounted using prolong antifade mounting reagent (Life Technologies, USA). Goat polyclonal Anti-HP1α (Abcam–ab77256) was used to label HP1 and visualized by chicken α-goat Alexa-647 (Life Technologies, USA) secondary antibody. Nesprin -2 was labelled using mouse Nesprin-2

antibody (a kind gift from Dr. Brian Burke, Institute of Medical Biology, Singapore) and visualized using goat α-mouse Alexa-647 (Life Technologies, USA), secondary antibody.1 All antibodies (except Nesprin-2) were used at 1:300 dilution. Nesprin-2 antibody was used at 1:10 dilution. F-actin was labelled by Rhodamine Phalloidin and Alexa-568 Phalloidin (Life Technologies, USA). G-Actin was labeled by DNase I conjugated to Alexa-488 (Life technologies, USA).

Mathematical modeling

There is a significant body of research suggesting that both cytoskeletal structures and nucleus are viscoelastic(1), so we model the mechanics of interconnected nucleus and cytoskeleton as a simple network of three spring-dashpot elements. The first, viscous, element represents the lamellar actin network; the second element, which is in parallel with the first one, is responsible for the actin-myosin stress fibres. The third spring-dashpot structure describes nuclear mechanics. We assume that the pre-stress force F_{pre} is generated by myosin and induces initial elongation of the cytoskeletal springs $X_c = F_{pre}/k_1$ and of the nuclear spring $X_n = F_{pre}/k_2$. In the model, we apply external force F_{appl} to the nuclear membrane as shown in Fig. 6a. Because of myosin-powered contraction, both nucleus and actin networks are pre-stressed effectively stretching the springs representing the stress fibers and nuclear elasticity. The direction of the external force pushing on the nuclear wall is such (Fig 7a) that it stretches the cytoskeleton further but relieves tension in the nucleus. The displacement of the nuclear membrane, *Z*, satisfies the equation:

$$\frac{dZ}{dt} = \frac{F_{appl} - (k_1 + k_2)Z}{(C_1 + C_2 + C_3)}.$$

We assume that after an average lag of $T_1 = 45$ seconds, the connection between the first cytoskeletal element (lamellar actin network) and nucleus breaks. After this break, the deformation of the nucleus is determined by the equation:

$$\frac{dZ}{dt} = \frac{F_{appl} + k_1(X_c - Z) - k_2(X_n + Z)}{(C_2 + C_3)}.$$

When the applied force ceases, parameter F_{appl} in the above equations becomes zero. We also assume that if the applied force persists for more than $T_2 = 90$ seconds, the link between the nucleus and stress fibers breaks as well, and the deformation of the nucleus is determined by the equation:

$$\frac{dZ}{dt} = -\frac{k_2}{C_3}Z.$$

Note, that the links' breaking could correspond to the observed plastic, irreversible changes within the nucleus (2, 3), rather than the links between actin cytoskeleton and nucleus. We

solved the equations above for long and short applied force pulses and computed the nuclear area. In both cases, for the first few tens of seconds the change of the nuclear area is very small due to very high viscosity of the actin network and respective slowly growing deformation. Then, some the actin-nuclear connections break and nuclear deformation accelerates. If the applied force is switched off fast enough, the area returns to roughly the original value (Fig. S15b). However, if the force is applied for a long enough time (Fig.S15a), all actin-nuclear connections break and the nuclear area gradually relaxes to the completely unstressed value. There is a very good agreement between the model predictions and the data indicating that the viscoelastic elements in the nucleus and cytoskeleton are responsible for instantaneous force sensing, while the viscous elements introduce characteristic time scales of tens of seconds allowing the cell to gauge not only the magnitude but also duration of the mechanical perturbations.

We model mechanochemical signaling assuming that the F-G-actin turnover in the cytoplasm is described by the following system of equations:

$$\frac{dG}{dt} = -\left(b_0 + b_1 F_{appl}\right) FG + aF, \quad \frac{dF}{dt} = \left(b_0 + b_1 F_{appl}\right) FG - aF$$

These equations are underlined by implicit assumptions that the F-actin network consists of multiple short actin filaments, certain fraction of which has uncapped barbed ends and growing with the rate proportional to the G-actin concentration. The number of such filaments is proportional to the total F-actin concentration, hence the term $\sim FG$. After capping, a filament disassembles completely into monomers with an average constant rate, hence the term $\sim aF$. When the external force is applied, we assume that the F-actin assembly increases(4), hence the factor $b_1 F_{appl}$ where $F_{appl} = 1$ if the external force is applied and $F_{appl} = 0$ if not. Both F- and G-actin concentrations are normalized to unity. In the model, we measure F:G ratio in the units of the inversed anisotropy, rather than of micromolar ratio. Similarly, all reaction rates are calibrated by this measure, rather than by micromolar concentrations. This is justified because experimentally we find the linear proportionality between the micromolar ratio and inversed anisotropy measures.The initial condition for this system is that before the force is applied, both F- and G-actin concentrations are in equilibrium. We solved numerically the actin turnover model equations and plotted the F- to G-actin ratio as a function of time (Fig. S15c). The model and the data agree well and illustrate that there is immediate, linearly growing shift from monomeric to F-actin in response to external force.

We model MKL transport as shown in Fig. 7a. All transport and dissociation rates are assumed to be the first-order reactions (5), while the MKL-G-actin association reactions are assumed to obey mass action kinetics. Respective system of equations has the form:

$$\frac{dM_c}{dt} = -\left(K_1 G + K_5\right) M_c + K_2 M_c^g, \quad \frac{dM_c^g}{dt} = K_1 G M_c + K_6 M_n^g - K_2 M_c^g$$

$$\frac{dM_n}{dt} = K_5 M_c - K_3 G_n M_n + K_4 M_n^g, \quad \frac{dM_n^g}{dt} = K_3 G_n M_n - K_6 M_n^g - K_4 M_n^g$$

Here M_c, M_n are the cytoplasmic and nuclear concentrations of MKL, M_c^g, M_n^g are also the cytoplasmic and nuclear concentrations of MKL, but associated with G-actin, and G and G_n are cytoplasmic and nuclear concentrations of G-actin; the reaction rates can be gleaned from Fig. 6a.Molar MKL concentration is much smaller than that of G-actin, so we do not include the G-actin transport in- and out- of the nucleus; the G-actin concentration in the cytoplasm is obtained from the F-G-actin dynamics model. The initial condition for this system is that before the force is applied, MKL concentrations in the cytoplasm and nucleus are in equilibrium and the mobility of MKL in the nucleus is significantly smaller than that of the cytoplasm (Fig.4d) suggesting possible interactions of MKL with the chromatin and its transcription factor SRF The numerical solution of this system plotted in Fig. S15d shows that the observed sigmoidal chemical response to the force with the characteristic time lag is the result of the multi-step biochemical relay (Fig. 7e), and thus the mechanochemical signalling is delayed relative to the mechanical sensing.

Supplementary Figures

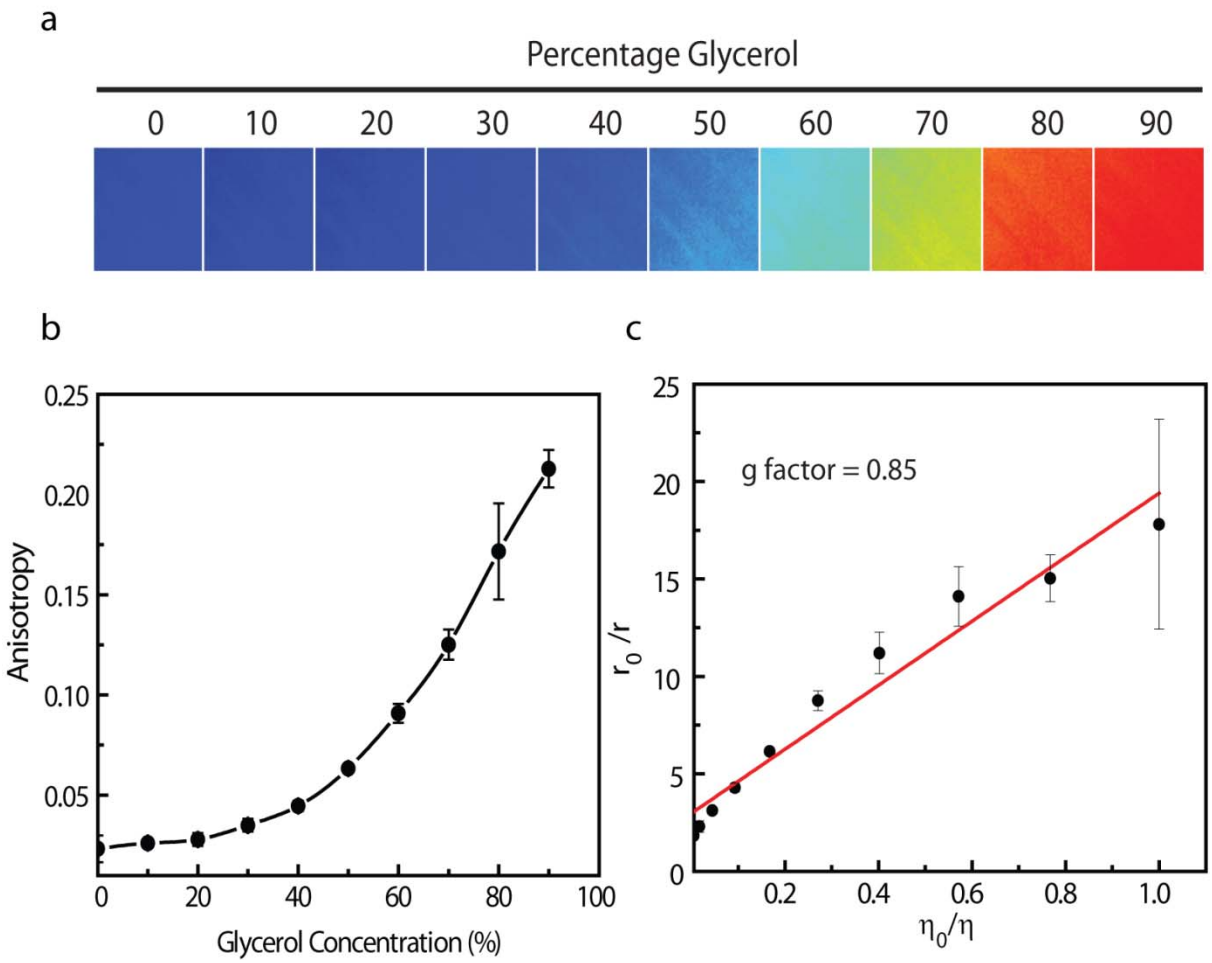

Fig S1.Calibration of fluorescence anisotropy.(**a**) Images showing fluorescence anisotropy of FITC in glycerol, with increase in the concentration of glycerol. (**b**) Plot showing increase in anisotropy with increase in glycerol concentration. (**c**) Perrin plot showing the variation of anisotropy with viscosity of glycerol. Error bars denote S.E.M.

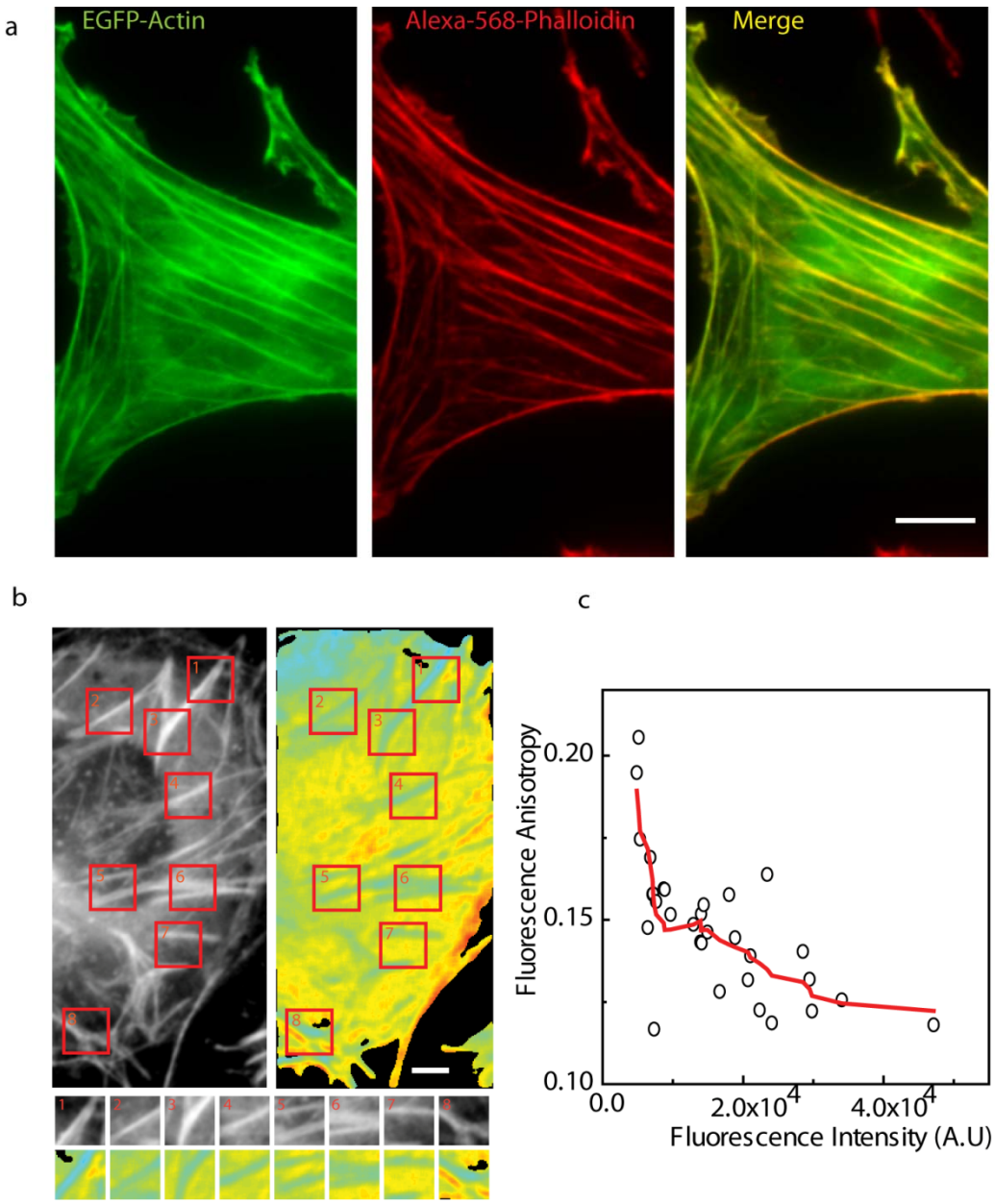

Fig S2. Actin stress fibers are marked by fluorescence anisotropy. (**a**) Representative image showing the expression of transfected EGFP actin and staining of endogenous actin by Alexa-568-Phalloidin. The merge image shows colocalization between the two images. (**b**) Representative image showing fluorescence intensity and anisotropy of EGFP-actin. The collage shows the enlarged images of regions showed by red ROI. Regions of low EGFP-actin correspond to high intensity in Intensity suggesting homoFRET. (**c**) Scatter plot between florescence intensity and fluorescence anisotropy showing an inverse relationship. Scale bar, 10 μm.

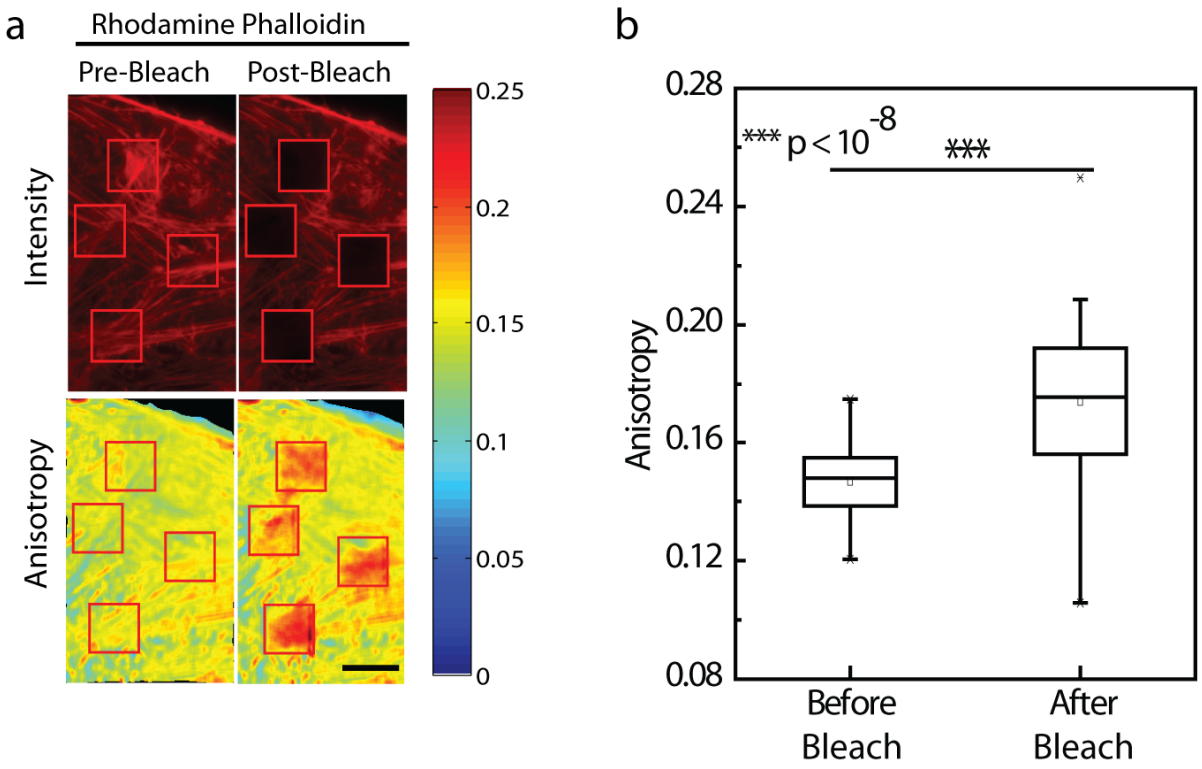

Fig S3. Characterization of homoFRET in EGFP-Actin by photobleaching (**a**) Intensity and anisotropy image of Rhodamine Phalloidin labelled HeLa cell before and after photobleaching. Red ROIs indicate the regions of photobleaching. (**b**) Box plot showing the increase in anisotropy of EGFP-actin upon photobleaching. Scale bar, 10μm.

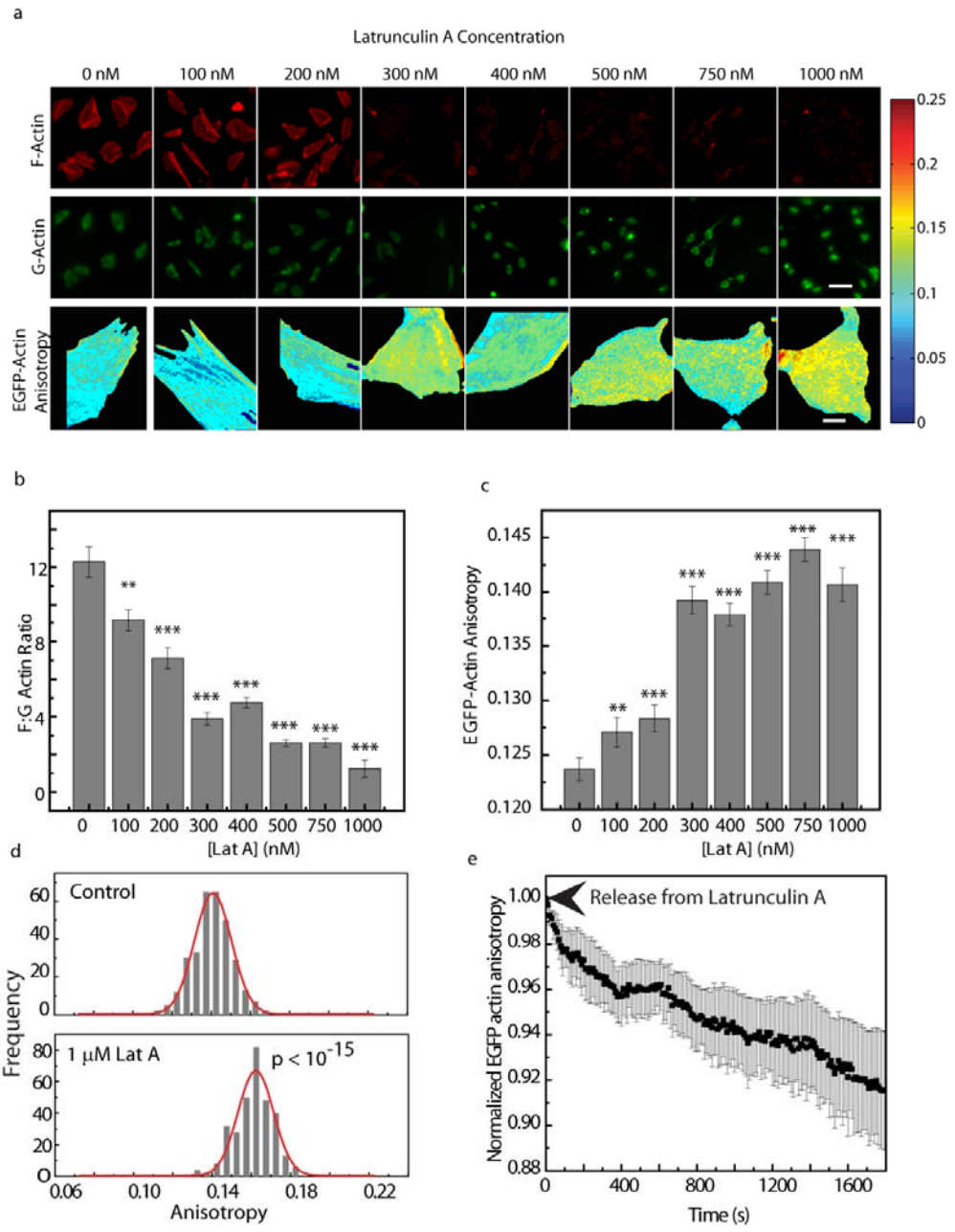

Fig S4. Characterization EGFP-actin anisotropy as a measure of F:G actin ratio. **(a)** Images showing intensity F-actin and G-actin, and EGFP-actin anisotropy with increasing concentration of Latrunculin A. (**b**) Bar plot showing decrease of F:G actin ratio with increase in Latrunculin A concentration. (**c**) Bar plot showing increase in EGFP-actin concentration with increasing Latrunculin A concentration. (**d**) Histogram showing increase in the anisotropy of EGFP-actin upon treatment with 1μm Latrunculin A. (e) decrease in EGFP-actin anisotropy upon release from Latrunculin A. Scale bar for F-actin and G-actin images, 50 μm. Scale bar for EGFP-actin anisotropy images, 10 μm. Error bars denote S.E.M. ** denotes $p < 0.05$ and *** denotes $p < 0.001$. T-test was performed between for comparison with control (0 nM Lat A).

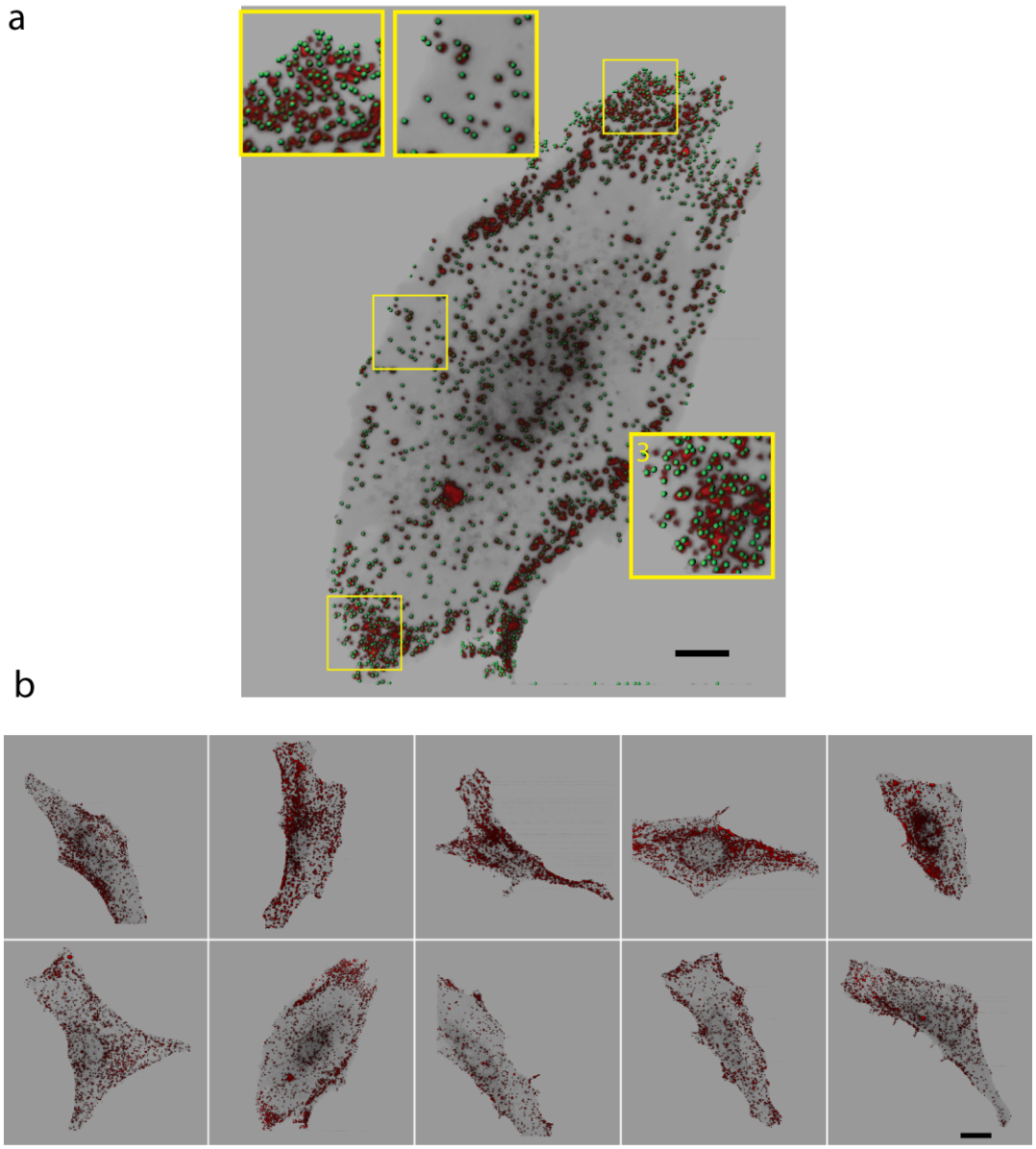

Fig S5.Distribution of beads on the surface of HeLa cells.(**a**) A representative image showing the distribution of 100 nm fluorescent carboxyl beads on the surface of the cells. Enlarged views of the regions marked by yellow ROI, shows the localization of the beads and the centre of the beads by green spots. (**b**) Collage of image showing that the beads are distributed uniformly over the surface of the cell. Scale bar, 10 μm

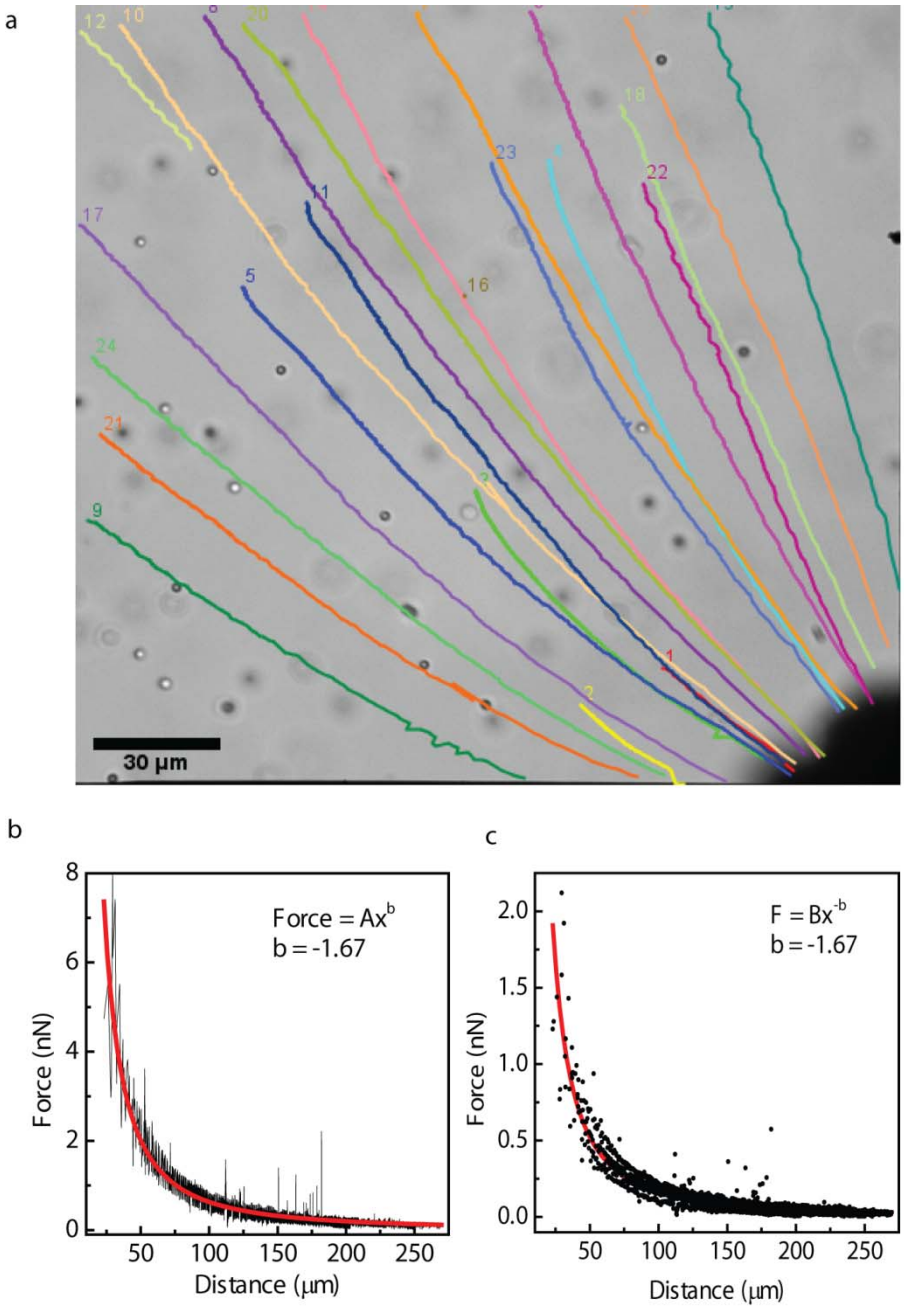

Fig S6. Calibration of force on cells. (**a**) Movement of 4 µm paramagnetic bead under the influence of external magnetic field produced using an electromagnet (black shadow in the bottom right corner). (**c**) Variation of force on the bead with increasing distance from the electromagnet. (**d**) Variation of force on a single cell computed from the variation of force on 4µm bead, magnetization of 4 µm and 100 nm beads and the number of 100 nm beads per cell.

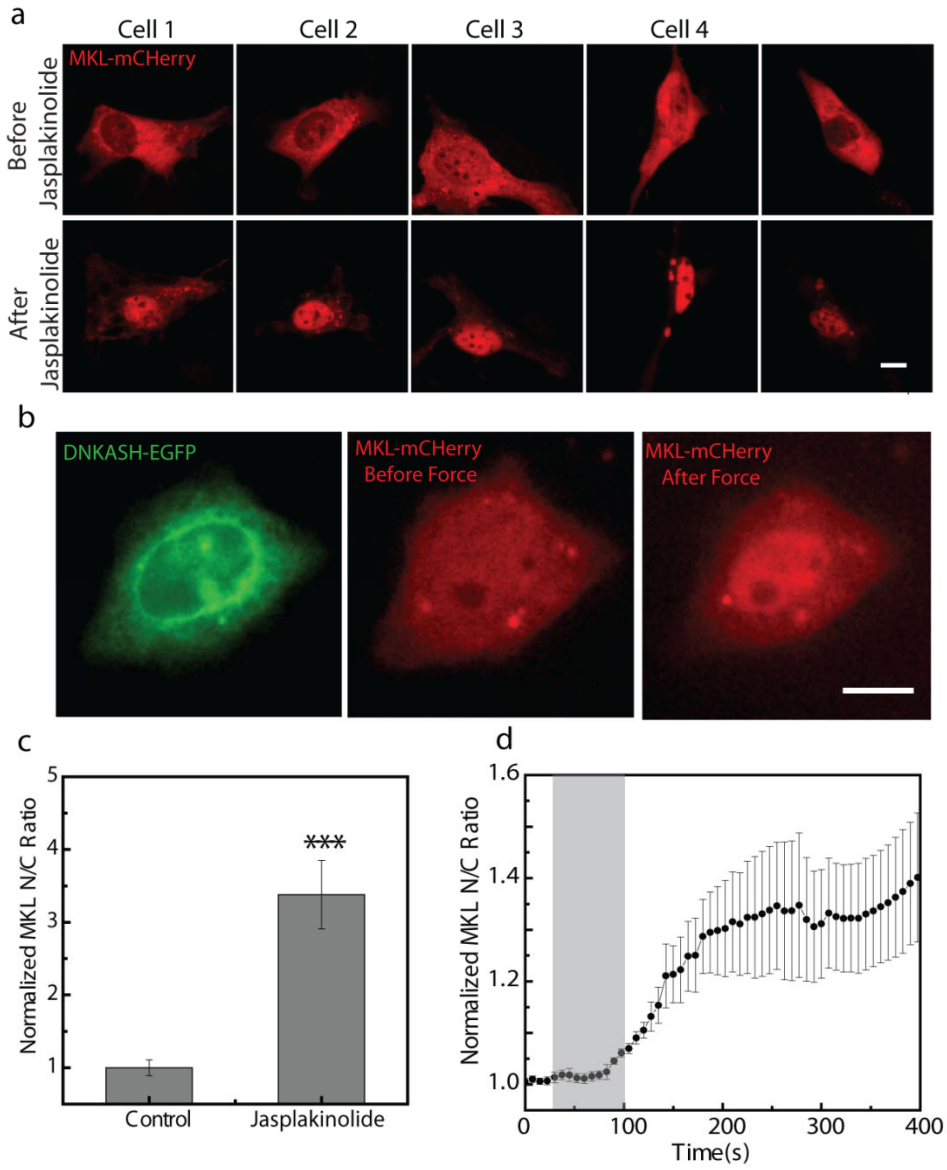

Fig S7. Effect of Jasplakinolide treatment and DNKASH-EGFP expression on MKL nuclear translocation. (**a**) Representative images of cells expressing MKL-mCherry before and after treatment with Jasplakinolide. (**b**) Representative images showing cells expressing DNKASH-EGFP and MKL-mCherry. Images of MKL-mCherry show nuclear translocation upon application of force. (**c**) Bar plot showing normalized MKL N/C ratio before and after treatment with Jasplakinolide. (**d**) Normalized MKL N/C ratio as a function of time upon application of pulse force. The duration of force is shown by gery ROI. Scale bar, 10 μm, Error bars indicate S.E.M. *** denotes $p < 0.001$.

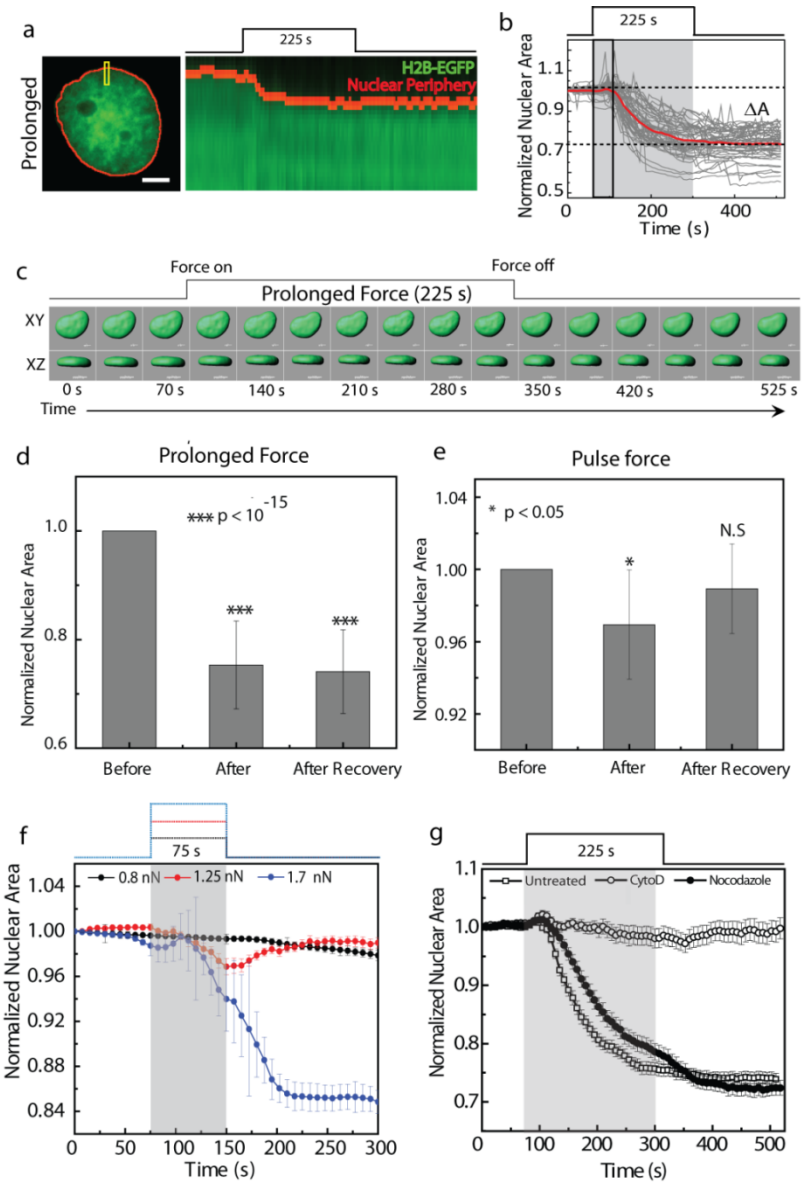

Fig S8. Nuclear deformation upon application of prolonged force. (**a**) Image showing a typical H2B-EGFP HeLa cell before application of force. Kymograph of the region shown by yellow ROI represents the deformation of the nucleus upon application of prolonged force. (**b**) Plot shows the change in normalized nuclear area due prolonged force application. (**c**) Time course images showing decrease in nuclear cross-sectional area and concomitant increase in nuclear height upon application of prolonged force. (**d**) Nuclear area before, during and after recovery from prolonged force. (**e**) Nuclear area before, during and after recovery from pulse force. (**f**) Plot showing normalized nuclear area as a function of time, upon variation of magnitude of the applied force. (**g**) Normalized nuclear area upon application of prolonged force in untreated cells and cells treated with Cytochalasin D and Nocodazole. Scale bar, 5 μm, error bars indicate S.E.M. *** denotes $p < 10^{-15}$ and * denotes $p < 0.05$.

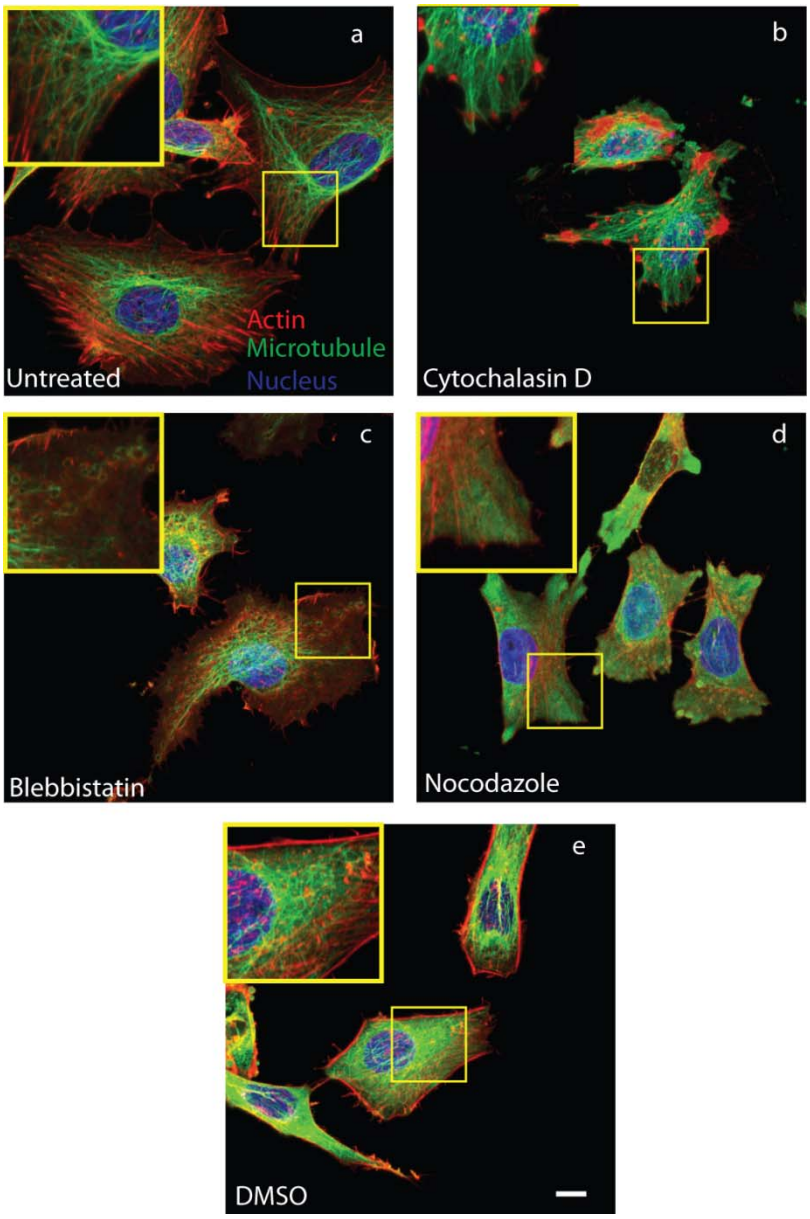

Fig S9.Drug concentrations used are sufficient for cytoskeletal perturbations. Actin microfilaments are visualized by staining with Rhodamine Phalloidin, microtubules are stained for α-tubulin and nucleus is labelled with Hoechst – 33342. (**a**) Untreated cells show intact actin and microtubule structure. (**b**) Treatment with 1 μM Cytochalasin D for 1 hr results in complete depolymerization of actin microfilaments. (**c**) 50 μM Blebbistatin treatment for 2.5 hrs shows significant loss of actin stress fibres. (**d**) 10 mg/ml Nocodazole treatment for 2.5 hrs leads to complete depolymerization of microtubules. (**e**) DMSO (used as a vehicle) treatment for 2.5 hrs did not show any significant change in actin and microtubule structure. Scale bar, 10 μm.

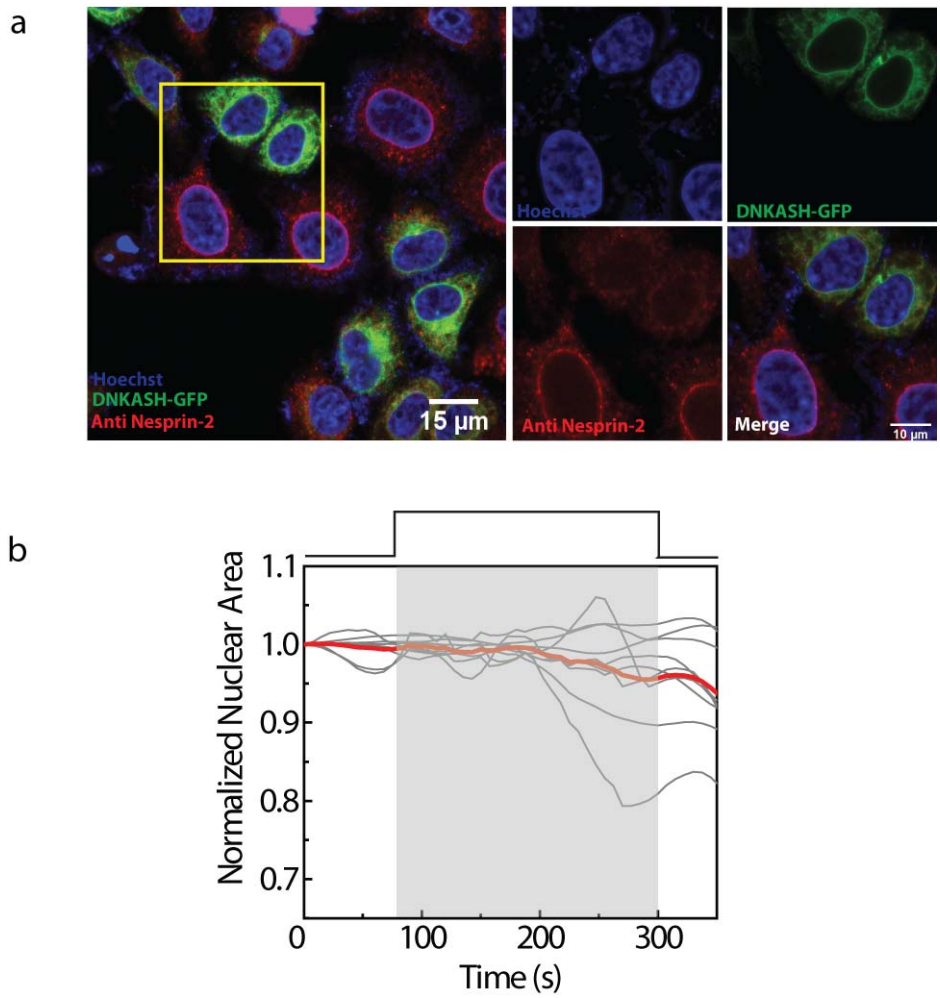

Fig S10. Changes in nuclear morphology LINC complex perturbation. (**a**) Field of view showing cells expressing dominant negative KASH. Region of interest shown in yellow is enlarged. DNA is shown in blue, DNKASH-GFP in green and Nesprin-2 antibody in red. Cells expressing DNKASH-GFP do not have Nesprin-2 expression around the nuclear periphery, but is displaced to the cytoplasm, whereas cells which do not express DNKASH-GFP have a well defined Nesprin-2 localization around the nucleus. (**b**) Force induced change in nuclear area of cells expressing DNKASH.

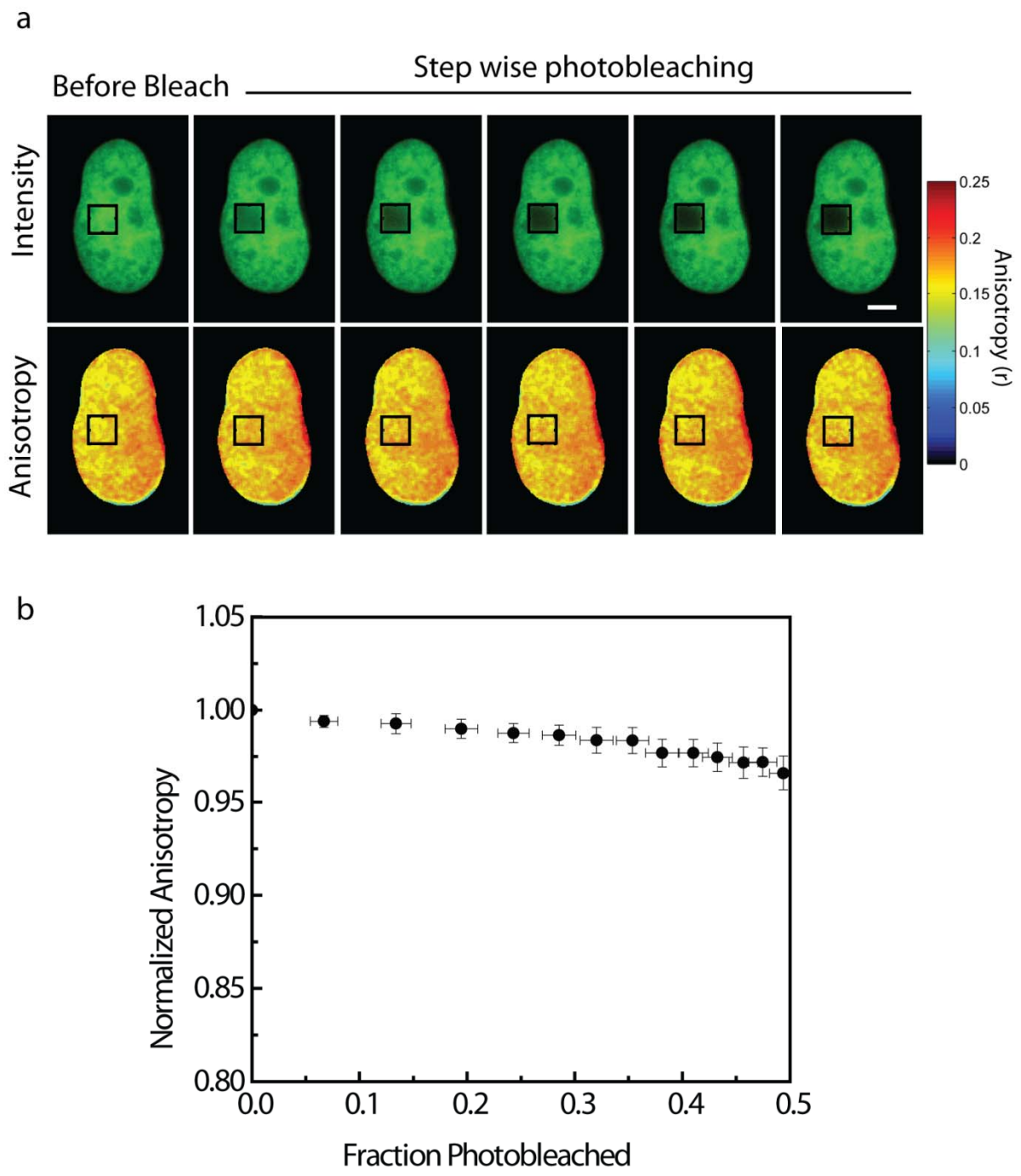

Fig S11. Absence of homoFRET in H2B-EGFP. (**a**) Collage of images showing intensity and anisotropy of H2B-EGFP upon photobleaching. (**b**) Plot showing the change in H2B-EGFP anisotropy as a function of fraction of photobleached molecules of H2B-EGFP. Scale bar, 5 μm.

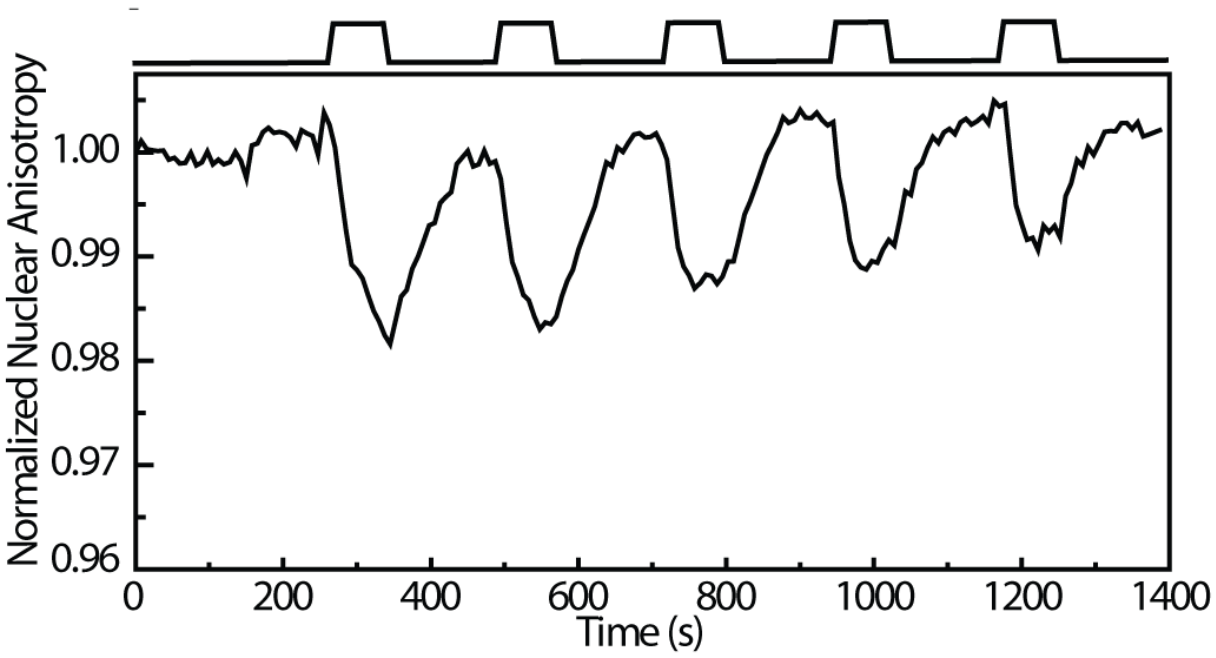

Fig S12. Changes in chromatin compaction upon multiple pulses of force. Plot shows the normalized nuclear anisotropy upon application multiple pulses of force. The nucleus responds similarly to each pulse of force.

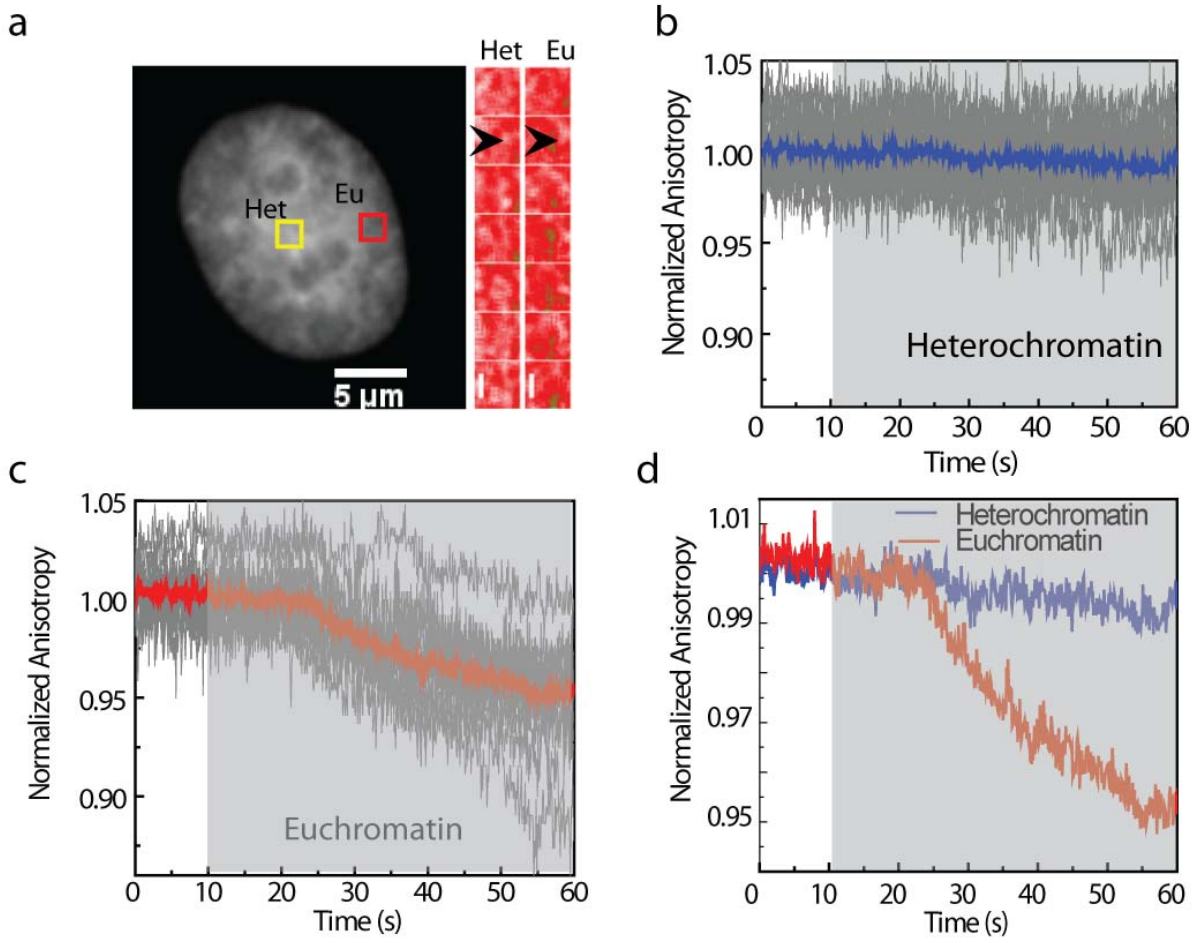

Fig S13. Force induced differential unravelling of chromatin (**a**) A typical H2B-EGFP-HeLa cell nucleus with euchromatin (red ROI) and heterochromatin (yellow ROI) regions marked. The collage shows force induced change in anisotropy of heterochromatin and euchromatin region. Force is applied from the image having a black arrow. (**b**) Force induced change in anisotropy at heterochromatin nodes. Grey traces indicate individual regions and blue indicates the mean response. (**c**) Force induced anisotropy change at euchromatin region. (**d**) comparison of the mean change in anisotropy at heterochromatin and euchromatin regions. Scale bar, 5 µm

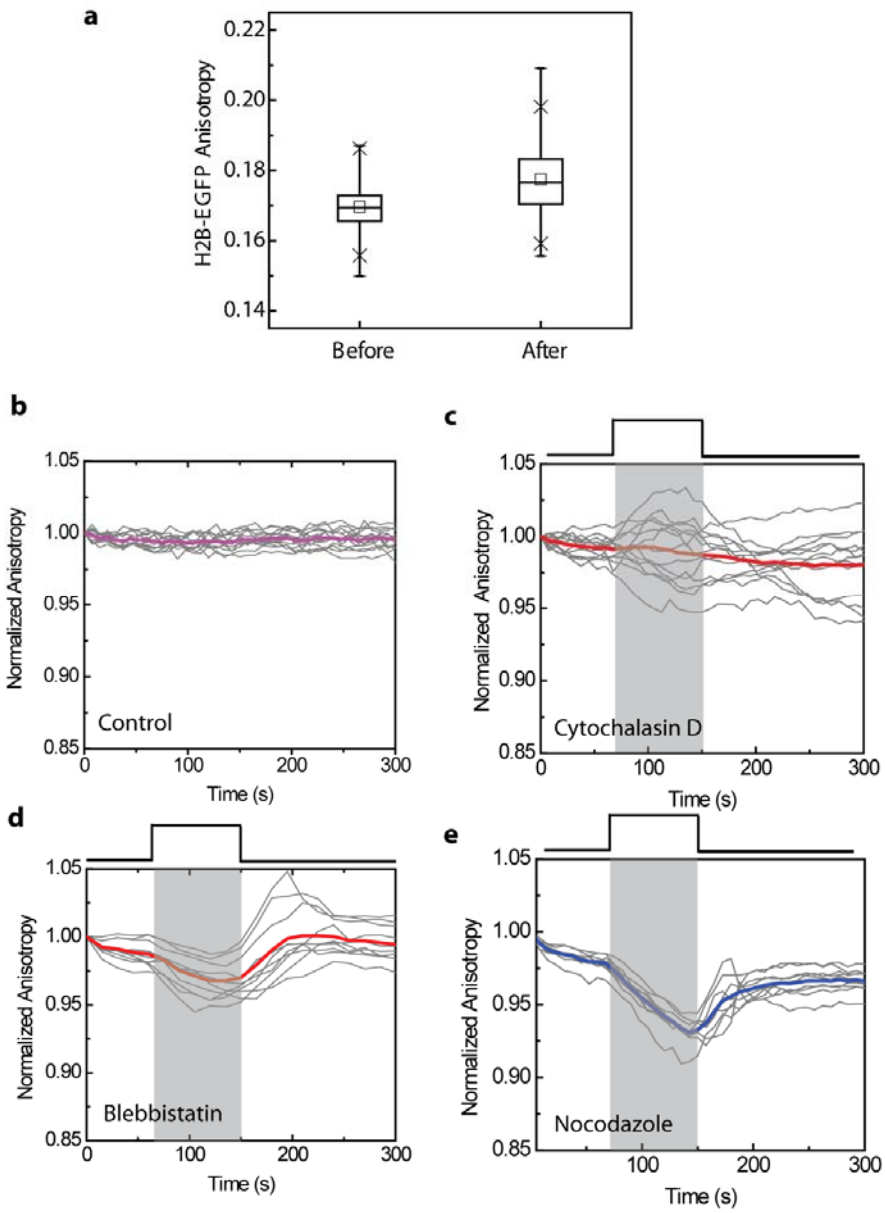

Fig S14. Force induced changes in chromatin compaction is dependent on actin cytoskeleton. (**a**) Anisotropy of H2B-EGFP, before and after treatment of Cytochalasin D indicate an increase in anisotropy of H2B-EGFP upon removal of prestress on the nucleus by actin depolymerization.(**b**) In control cells, when no force was applied, no significant change in the anisotropy of H2B-EGFP was observed. (**c**) Upon treatment with Cytochalasin D, no decrease in the anisotropy of H2B-EGFP is observed. (**d**) When cells were treated with Blebbistatin a decreased change in anisotropy was observed as compared to the untreated cells shown in Fig 2. (**e**) Nocodazole treatment does not alter the response of the nucleus towards application of force suggesting that it is not involved in force induced chromatin reorganization.

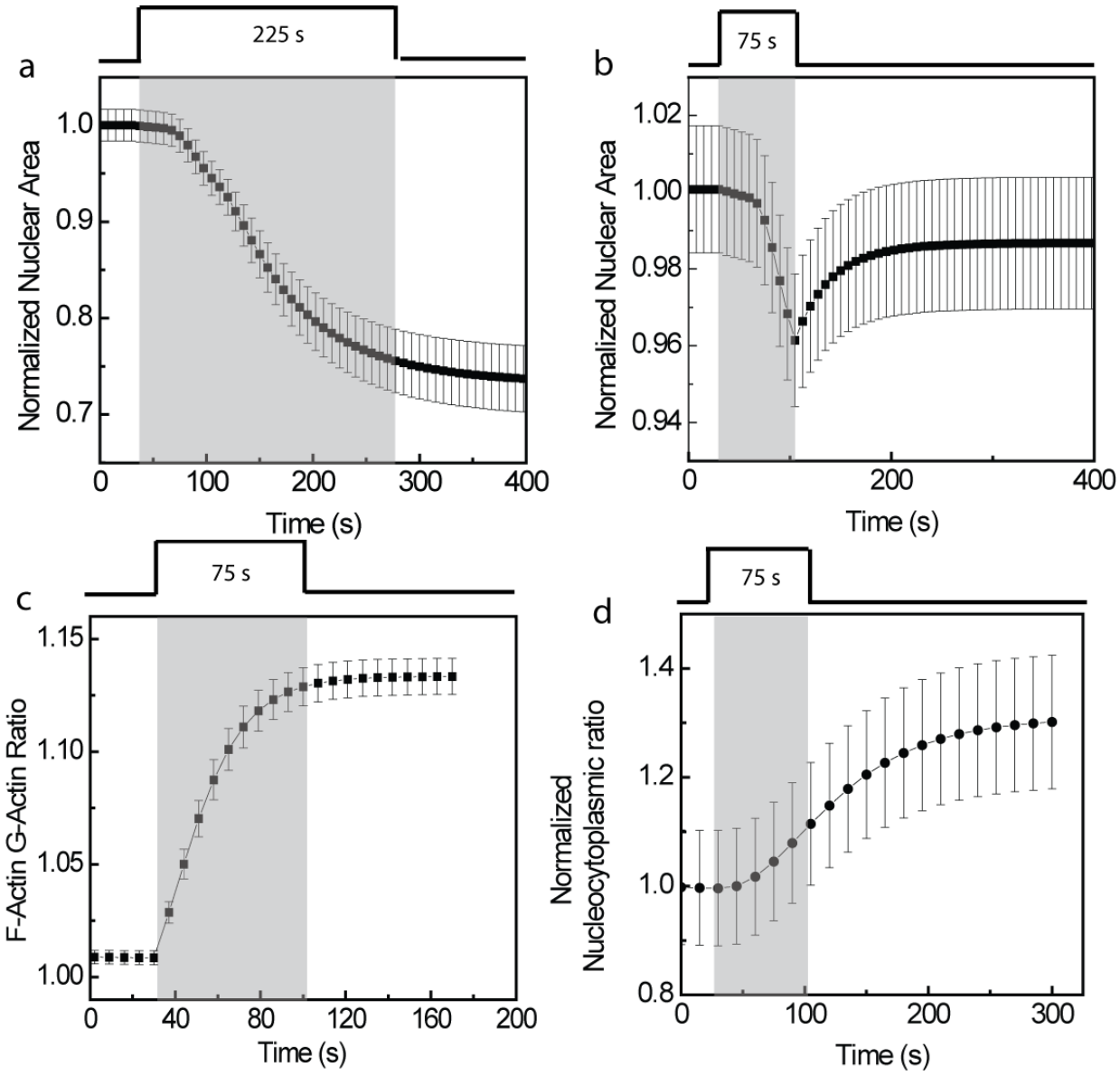

Fig S15. Theoretical modelling of the mechanotransduction process. (**a**) Simulated curve for the change in nuclear area upon application of prolonged force and (**b**) pulse force. F-Actin G-Actin ration is modelled in (**b**) and the MKL response is modelled in (**d**). Error bars indicate the square root of the variance of 20 simulations in which model variables were randomly varied by 30 %.

Term	Description	Units
Z	Nuclear deformation	mm
F	F-actin concentration	Dimensionless units
G	G-actin concentration	Dimensionless units
M_c	Cytoplasmic MKL concentration	Dimensionless units
M_n	Nuclear MKL concentration	Dimensionless units
M_c^g	Cytoplasmic MKL-G-actin concentration	Dimensionless units
M_n^g	Nuclear MKL-G-actin concentration	Dimensionless units
F_{pre}	Prestress force	2.5 nN
F_{appl}	Applied force	1.25 nN
k_1	Stress fiber spring constant	5 nN/μm
k_2	Nuclear spring constant	5 nN/μm
C_1	Actomyosin network viscous drag	7.5×10^3 nN×sec/μm
C_2	Stress fiber viscous drag	3.75 nN×sec/μm
C_3	Nuclear viscous drag	375 nN×sec/μm
T_1	Average life-time of actin network – nucleus links	45 sec
T_2	Average life-time of stress fiber – nucleus links	90 sec
a	Actin disassembly rate	0.3/30 sec
b_0	Actin assembly rate	0.3/((unit of [G])×(30 sec))
b_1	Force-dependent actin assembly rate	0.04/((unit of [G])×(30 sec))
G_n	Nuclear G-actin concentration	1 unit of [G]
K_1	Cytoplasmic rate of MKL-G-actin association	2/((unit of [G])×(30 sec))
K_2	Cytoplasmic rate of MKL-G-actin dissociation	3/30 sec
K_3	Nuclear rate of MKL-G-actin association	0.7/((unit of [G])×(30 sec))
K_4	Nuclear rate of MKL-G-actin dissociation	0.7/30 sec
K_5	Rate of cytoplasm-nucleus MKL transport	0.3/30 sec
K_6	Rate of nucleus- cytoplasm MKL-G-actin transport	0.7/30 sec

Table S1: The table describes the parameters used in modelling the mechanotransduction from plasma membrane to the nucleus.

References

1. J. S. Lee, C. M. Hale, P. Panorchan, S. B. Khatau, J. P. George, Y. Tseng, C. L. Stewart, D. Hodzic, D. Wirtz, Nuclear lamin A/C deficiency induces defects in cell mechanics, polarization, and migration. *Biophys J* 93, 2542 (2007).

2. J. D. Pajerowski, K. N. Dahl, F. L. Zhong, P. J. Sammak, D. E. Discher, Physical plasticity of the nucleus in stem cell differentiation. *Proc Natl Acad Sci U S A* 104, 15619 (2007).

3. K. N. Dahl, A. J. Engler, J. D. Pajerowski, D. E. Discher, Power-law rheology of isolated nuclei with deformation mapping of nuclear substructures. *Biophys J* 89, 2855 (2005).

4. S. Deguchi, M. Sato, Biomechanical properties of actin stress fibers of non-motile cells. *Biorheology* 46, 93 (2009).

5. M. K. Vartiainen, S. Guettler, B. Larijani, R. Treisman, Nuclear actin regulates dynamic subcellular localization and activity of the SRF cofactor MAL. *Science* 316, 1749-1752(2007).